Optical and Quantum Electronics (2020) 52:249
https://doi.org/10.1007/s11082-020-02381-x

Investigation on the effects of laser parameters on the plasma profile of copper using picosecond laser induced plasma spectroscopy

Mohamed Fikry[1,2] · Walid Tawfik[3] · Magdy M. Omar[1]

Received: 29 February 2020 / Accepted: 27 April 2020 / Published online: 2 May 2020

Abstract
Laser induced plasma generation and characterization, affected by laser parameters and sample physical properties, represent important phenomena in many fields of applications. In this work, we present new studies on the effects of an appropriate combination of laser wavelengths and pulse energies on the generated plasma characterization using a single shot picosecond Nd:YAG laser. The plasma plume of a pure copper sample has been generated by laser induced plasma spectroscopy (LIPS) using a single shot 170 ps laser pulse with wavelengths (266, 355, 532 and 1064 nm) and varying laser fluence (10–41 J/cm^2). The spectral intensities of Cu I 324.75, 327.39, 515.32 and 521.82 nm have been observed. The plasma electron temperature and density have been determined from the Boltzmann plots and Stark-broadening profiles of the plasma spectral lines, respectively, assuming the local thermodynamic equilibrium (LTE) condition. It has been found that the electron temperature and electron density values increase from around 10,000 to 20,000 K and around 2×10^{17} to 1.5×10^{18} cm^{-3}, respectively, with the increase in the laser wavelength and pulse fluence gradually. These observations can be understood due to the variations of mass-ablation rates, inverse-Bremsstrahlung, and photo-ionization with the studied pulse wavelength and pulse energy. The obtained results explore the opportunity to control specific generated plasma parameters by applying proper picosecond pulse parameters which can be considered in many fields of material science spectroscopic analysis and control the plasma interaction dynamics.

Keywords Picosecond · Laser induced plasma spectroscopy · LIPS · Plasma plume · Copper · Electron temperature · Electron density · Boltazmsan plot · Stark-broadening · LTE

✉ Walid Tawfik
walid_tawfik@niles.edu.eg

[1] Department Physics, Faculty of Science, Cairo University, Cairo, Egypt

[2] Egypt Nanotechnology Center (EGNC), Cairo University, Cairo, Egypt

[3] National Institute of Laser Enhanced Sciences (NILES), Cairo University, Cairo, Egypt

1 Introduction

Plasma can be generated by the extreme change in a matter temperature to overcome the binding electrostatic forces between its electrons and nucleus (Eddington 1988). Consequently, a hot gas is therefore composed of a mixture of neutral atoms, electrons and ions (Adhikari and Khanal 2013). Plasma radiation relies on the features of the isolated radiation kinds and the radiator's immediate surroundings. This dependence on the plasma properties is a consequence of the fact that ions and electrons interact with other species through the long-range of Coulomb potential (Cooper 1966). Plasma spectroscopy is an essential diagnostic method in plasma processing and technology as well as in basic studies including astrophysics and plasma physics. The most useful classifications for plasmas are distinguished into two main groups according to their temperature i.e., the high-temperature or fusion plasma and the low temperature or gas discharge (Fantz 2006). Firstly, a high temperature plasma state in which, electron temperature (T_e), ionic temperature (T_i) and gas temperature (T_g) assumed to be equally where its plasma temperature (T_p) values ranged 10^6–10^8 K and its plasma electron density (N_e) around 10^{20} cm^{-3}. Secondly, a low-temperature plasma can be divided into two types; thermal plasma or hot plasma and non-thermal plasma or cold plasma state. In hot plasma state N_e reaches 10^{20} cm^{-3} and $T_e \approx T_i \approx T_g$ with T_P fluctuate from 10^3 to 10^4 K while in cold plasma state N_e less than 10^{19} cm^{-3} as low as 10^{10} cm^{-3} with relatively low-temperature T_P ranged from 300 to 10^3 K where $T_e >> (T_i \approx T_g)$ (Asenjo-Castillo and Vargas-Blanco 2016). If the plasma temperature decreased from 300 K down to 1 K then it is called ultracold plasma which can be generated in vacuum by photo–ionizing laser-cooled atoms (Killian and Rolston 2010).

Using a laser beam to induced material breakdown is one of the most important plasma production techniques, by focusing a high energy laser pulse on any target material (solid, liquid, or gas). The produced radiation can lead to rapid, local heating, intense evaporation, and degradation of the material at the focal point (Conrads and Schmidt 2000). The interaction between the laser beam and the material depends on the mechanical, physical and chemical features of the target, as well as on the properties of the laser such as the laser wavelength, intensity fluence and the pulse width (Thiem et al. 1994).

Optical emission spectroscopy is one of the common techniques used for plasma diagnosis and can give information about the sample chemical composition in addition to plasma characteristics. Laser-generated plasma irradiates emission-spectra of various types, mostly extent from ultraviolet to visible and infrared regions. The technique which based on the spectroscopic analysis of laser generated plasma optical emissions frequently known as laser induced plasma spectroscopy (LIPS) or laser induced breakdown spectroscopy (LIBS) (Rusak et al. 1997). The technique is suitable for quick and online basic assessment of all material phases (Baskevicius et al. 2016). LIPS efficiently used to evaluate the presence target's trace components with conventional calibration and creative calibration-free methods (Gondal and Dastageer 2014). Due to growing concern about real-time (online) scanning, the field of LIPS has evolved rapidly as a consequence of a wider spectrum of applications and recent developments for LIPS analytical technologies in the trade. LIPS can be utilized quickly in laboratory, industry, in-situ, in stand-offs up to over 110 m, as sample preparation is not necessary for LIPS (Tawfik 2015).

Over the last ten years, ultrafast laser light has been a hot subject of studies extend from picosecond to femtosecond laser pulse applications (Jarota et al. 2019). The considerations of picosecond lasers include optical coherence tomography, new solutions for optical communications and laser ultrashort pulse management. The processing of ultrafast laser

materials provides various advantages over conventional procedures: a quick, accurate and versatile technique, due to the electron-phonon interaction and quicker vaporization of the target martial than energy transferred throughout the surrounding areas (Phillips et al. 2015; Sugioka 2017). For picosecond laser pulses, it has been previously shown that picosecond pulses induce plasma ablation with reduced heat-affected zone and less heat dissipation compared to nanosecond pulsed laser ablation. By the end of these ultrafast picosecond laser pulses, the electron energy distribution generally archives an equilibrium state. These effects are due to the duration of the whole process is in the range of the electron-lattice relaxation time, which is typically in the picosecond regime for metal targets (Ding et al. 2011; Tan et al. 2018).

LIPS is affected by laser pulse parameters, which have been studied by several scientists to reveal the plasma evaluation. Kompitsas et al. (2000) used the LIPS technique to analyze environmental samples using nanosecond pulsed Nd:YAG laser at NIR(1.064 μm) and UV (355 nm) with varied pulse energy from 10 to 50 mJ. They concluded that, the quality of the spectra depends on the various experimental parameters. Abdellatif and Imam (2002) studied the plasma laser parameters achieved by the nanosecond Nd:YAG laser at varying laser wavelengths (1064, 532 and 355 nm) with different laser pulse energies (60, 100 and 500 mJ) for aluminum plates at different focusing lengths. They determined that, the maximum value of the T_e was found at a certain distance away from the target surface depending on the laser wavelength whereas, the N_e reaches its highest value near the target surface. Fornarini et al. (2006) considered a range of fluencies 50–250 J/cm^2 of Nd:YAG laser wavelengths 1064 and 355 nm with pulse duration 8 ns based on the analytical outcomes acquired from the use of LIPS diagnostics of bronze plasma. They inferred that; more limited thermal effects are expected if a laser with a shorter wavelength is considered. Unnikrishnan et al. (2010) investigated the time-resolved Nd:YAG laser operated at 355 nm, pulse width of 6 ns, repetition rate of 10 Hz and laser pulse irradiance of 4.5×10^8 W/cm^2 to induce Cu plasma spectroscopy of neutral atom and ion line emissions at atmospheric pressure. They indicated that, the optimum delay time is considered from the temporal evolution of the intensity ratio of two Cu I lines, assuming plasma optically thin and LTE conditions necessary for the LIPS analysis of samples. Naeem et al. (2013) group measured the pure copper plasma parameters applying a 532 nm Nd:YAG pulsed laser with a pulse duration of 5 ns and 10 Hz repetition rate at pulse energies of 17.6 and 88.6 mJ. They concluded that, a direct relationship between the plasma parameters and the laser irradiation whereas they were inverse to the distance from the sample surface. Messaoud Aberkane et al. (2015) determined the effect of 50 mJ Nd:YAG laser wavelengths 1064, 532 and 355 nm at 7, 9 and 10 ns pulse duration in air at atmospheric pressure on the correlation between T_e and surface hardness of Fe–V–C metallic alloys. They decided that, the surface hardness measurement using LIPS is more efficient by applying excitation laser in the NIR than in the UV. Asamoah and Hongbing (2017) studied the effect of variations in laser energy 150, 250 and 350 mJ of the nanosecond Nd:YAG laser source of 1064 nm at 1 Hz repetition rate and 10 ns duration pulse width used to investigate the plasma T_e of Mg. They found that, the T_e values of the Mg plasma increase rapidly with increasing laser energy. Recently, the ultrafast femtosecond laser with pulse wavelength 800 nm, pulse duration of 50 fs and 1.9 mJ laser energy, was used to generate a high T_e and low N_e plasma with strong spectral intensity by changing the space between the focusing lens and the sample surface in the LIPS configuration (Xu et al. 2019). They found that, the plasma condition at high T_e and low N_e can be used to improve the spectral resolution of LIPS. It can be inferred from these previous considerations that most of them have studied the effects of only one or two laser parameters on the plasma profile using nanosecond laser

pulses while most of the ultrafast studies focus on one laser parameter only, i.e. rare studies considered the effects of different wavelengths and energies under the regime of ultrafast pulses especially picosecond pulses.

In this work, we aim to apply the picosecond laser induced plasma spectroscopy to investigate the produced copper plasma profile. The emission lines of LIPS spectra are studied in the visible region. The combined effects of different laser wavelengths and laser pulse energies on the plasma plume electron temperature and electron density were considered. We intentionally try to control a specific region of plasma temperature and electron density by controlling the parameters of a picosecond laser plus.

2 Material and methodology

2.1 Material

A solid sample of a pure metal copper disk (K. J. Lasker Ltd., USA, purity of 99.99%) with a diameter of 3 cm and thickness 0.25 cm is used as a target sample.

2.2 X-ray diffraction sample analysis

The purity of Cu disk is confirmed by the X-ray diffraction (XRD) analysis carried out used the Bruker instrument model D8 discover advanced diffractometer (Germany). The instrumental parameters were set as follows: Cu-K_α graphite monochromator radiation, 40 kV, electrical current 30 mA, and 2θ range with a scanning speed of 1° per minute from 5° to 80°.

2.3 Experimental LIPS setup

The schematic diagram of the used LIPS setup is shown in Fig. 1, where an ultrafast picosecond Nd:YAG pulse laser, instead of nanosecond laser was used in the LIPS setup as described previously in detail elsewhere (Aslam Farooq et al. 2013; Qindeel and Tawfik 2014). Briefly, in this experiment, the plasma was produced using a picosecond Q-switched Nd:YAG laser (SL334, Eksapla, Lithuania) at four laser wavelengths (L_λ) 266 nm (UV), 355 nm (UV), 532 nm (Vis) and 1064 nm (NIR) at repetition rate 1–5 Hz and pulse

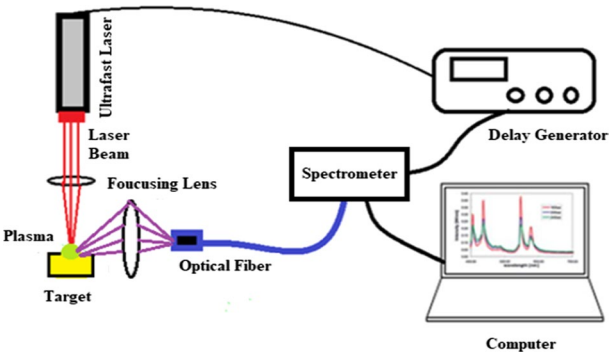

Fig. 1 A schematic diagram of the LIPS system

duration from 500 to 170 ps. A laser power meter (model 11 Maestro, Standa LTD. Lithuania), was used to monitor the energy for each laser pulse with accuracy ±1%.

In the current experimental setup, the wavelengths of the Nd:YAG (L_λ) (266, 355, 532 and 1064 nm) were operated at different energies in the range from 20 to 80 mJ ± 5%. The laser beam fluencies varied gradually from 10 to 41 J/cm^2 at 170 ps pulse duration for single-shot pulses are used. A plane–convex quartz lens with 150 mm focal length was used to focus the laser beam on the Cu disk target with a spot size of about 0.5 mm ± 0.1 mm to produce the plasma plume, where the diameter of the spot was adjusted by changing the distance between the laser lens and the target. The copper target was placed on x–y scanning stage to provide refresh sample material for each laser pulse to minimize errors. A Plano-convex quartz lens with 100 mm focal length was adjusted to the center of the plasma plume to collect the plasma emission at position 90° to the laser axis. Then the collected emission was transferred to an Ocean Optics spectrometer (HR4000 UV–NIR, from 200–1100 nm) using an optical fiber with 400 µm core diameter. The delay time between the laser pulse Q switch and the spectrometer detection was adapted to 1 µs and the integration time was optimized at 10 µs, which was considered as the optimum delay to obtain LTE plasma hypothesis as found before (Aslam Farooq et al. 2013; Qindeel and Tawfik 2014).

3 Results and discussion

3.1 Result of X-ray diffraction sample analysis

The X-ray diffraction (XRD) measurement pattern of the copper target is shown in Fig. 2.

The XRD pattern in Fig. 2 of the Cu target represents three characteristics peaks observed at 43.8°, 50.9° and 74.6° that referred to (111), (200) and (220) planes of Cu, respectively. These planes of Cu confirm a pure cubic phase of fcc structure (JCPDS No.85–1326) (Sahai et al. 2016; Dong et al. 2018).

3.2 LIPS spectrum studies

The qualitative compositional analysis of the Cu target is achieved from the optical emission spectrum of the laser produced plasma created on its surface using an ultrafast picosecond

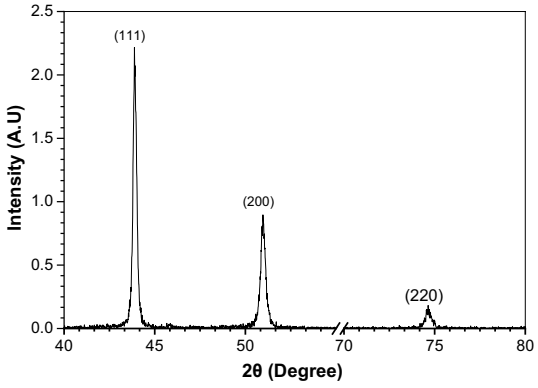

Fig. 2 XRD pattern of a pure Cu target

Nd:YAG pulsed laser, fluence gradually from about 10 to 41 J/cm^2. Figure 3a–d represents the LIPS emission spectra of the Cu sample covering the wavelength ranges 250–550 nm at different laser wavelengths 266, 355, 532 and 1064 nm. All the spectra were recorded under identical experimental conditions. This spectral region is selected because it gathers the highest Cu emission lines intensities which should be under optically thin and plasma in LTE as crucial conditions for the measurements of plasma parameters. The four selected strong lines of singly ionized copper are Cu I 324.75, 327.39, 515.32 and 521.82 nm due to the transitions ($3d^{10}4p,\ ^2P_{3/2} \rightarrow 3d^{10}4s,^2S_{1/2}$), ($3d^{10}4p,\ ^2P_{1/2} \rightarrow 3d^{10}4s,^2S_{1/2}$), ($3d^{10}4d,\ ^2D_{3/2} \rightarrow 3d^{10}4p,^2P_{1/2}$) and ($3d^{10}4d,\ ^2D_{5/2} \rightarrow 3d^{10}4p,^2P_{3/2}$), respectively.

The characteristics and transitions of the selected Cu emission lines have been identified with the help of the NIST database as shown in Table 1, where these data used to calculate the plasma plum parameters (Kramida and Ralchenko 2019).

Figure 4 demonstrates the increase in the signal to noise (S/N) ratio for both spectral lines 324.75 and 327.39 nm at showed the same trend with a decrease of L_λ at the same laser pulse energy. It has been recognized from Figs. 3 and 4, that the behavior of increment of both of the Cu emission spectral intensity and S/N ratio with the decrement of the laser wavelengths. This profile can be understood since photon energy increases for shorter L_λ that results in a high mass-ablation rate of copper. Consequently, more free electrons, ions and excited atoms are generated and cause an increment in the plasma emission intensity i.e. improve the S/N ratio (Murbat 2017; Safeen et al. 2019). Similar behavior due to the effect of varying the laser

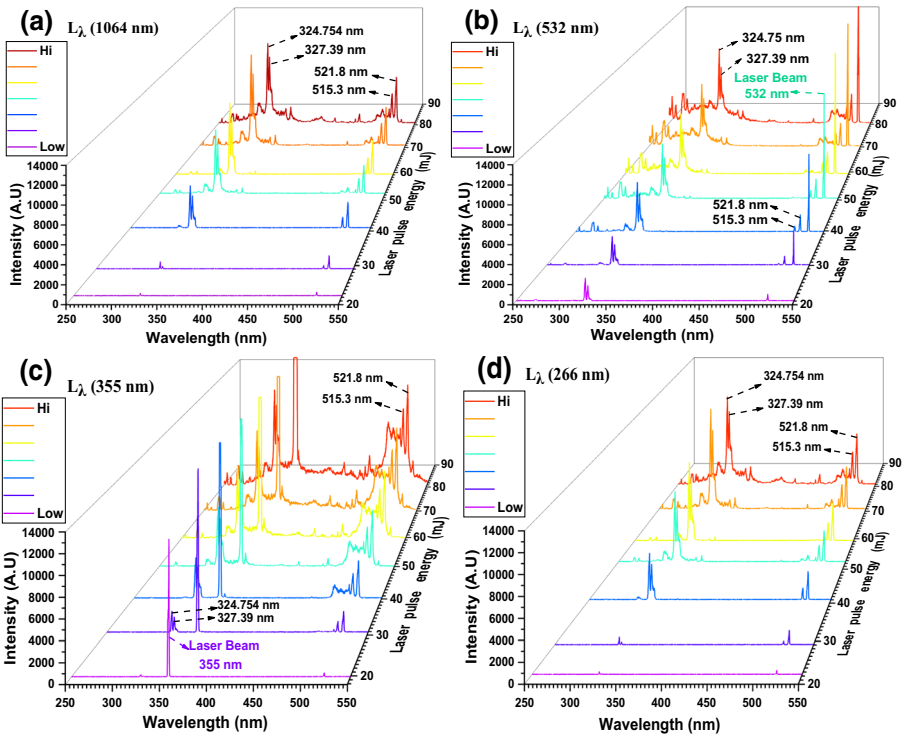

Fig. 3 LIPS emission spectra of Cu target using laser pulse energies from 20 to 80 mJ at different laser wavelengths (L_λ) **a** 1064 nm, **b** 532 nm, **c** 355 nm and **d** 266 nm

Table 1 Spectroscopic parameters of the emission lines of Cu I used to calculate the plasma parameters, taken from NIST database (Kramida and Ralchenko 2019)

Wavelength (nm) of Cu I	Transitions			Transition probability (A_{ki}) (10^7 s^{-1})	Energies (eV)			g_k
	Upper level		Lower level		E_k	E_i	ΔE	
324.75	$3d^{10}4p$, $2P_{3/2}$	→	$3d^{10}4s$,$^2S_{1/2}$	13.95	3.816	0	3.816	4
327.39	$3d^{10}4p$, $2P_{1/2}$	→	$3d^{10}4s$,$^2S_{1/2}$	13.76	3.785	0	3.785	2
515.32	$3d^{10}4d$, $2D_{3/2}$	→	$3d^{10}4p$,$^2P_{1/2}$	6.00	6.191	3.785	2.406	4
521.82	$3d^{10}4d$, $2D_{5/2}$	→	$3d^{10}4p$,$^2P_{3/2}$	7.50	6.192	3.816	2.376	6

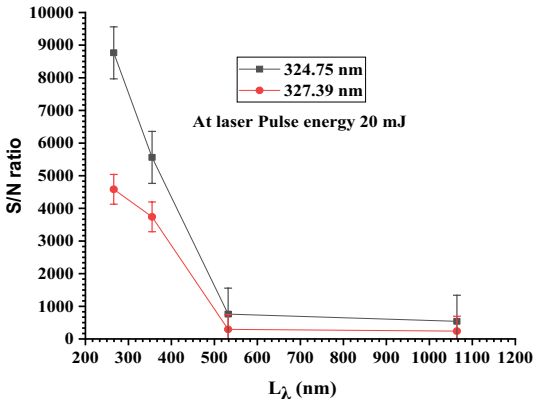

Fig. 4 Variation the signal to noise (S/N) ratio of the observed LIPS emission spectral lines, **a** Cu I 324.75 nm and **b** Cu I 327.39 nm, using different laser wavelengths (L_λ) at a laser pulse energy of 20 mJ

wavelength on the observed S/N ratio was reported by Kompitsas et al. (2000); Abdellatif and Imam (2002).

3.3 Plasma parameters and LTE considerations

To provide accurate consideration of LIPS plasma parameters, the local thermodynamic equilibrium and optically thin plasma conditions are assumed in which case the emissions from electron collisions are much larger than from the radiative processes (Gojani 2012). For optically thin plasma at LTE, the re-absorption effects of plasma emission are negligible (Liu et al. 1999). So, the spectral line intensity is a measure of the population of the corresponding energy level of an element in the plasma (Gojani 2012).

3.3.1 Measurement of plasma temperature

Under the above-assumed LTE, conditions, the plasma temperature is considered from the emission lines intensities of Cu applying Boltzmann plot method (Liu et al. 1999), which is given by;

$$I = \frac{C F}{\lambda} \frac{A_{ki}\, g_k}{U(T)} \exp\left(-\frac{E_k}{K T_e}\right) \quad (1)$$

The natural logarithm of Eq. 1, gives

$$\ln \frac{I\,\lambda}{A_{ki}\,g_k} = -\frac{1}{KT_e}E_k + \ln \frac{C\,F}{U(T)} \tag{2}$$

where I is the intensity of the spectral line, λ is the wavelength of the spectral line, K is the Boltzmann constant, U(T) is the partition function, A_{ki} is the transition probability, g_k is the statistical weight for the upper level, E_k is the exciting level energy, T_e is the electron temperature, F is an experimental factor and C is the species concentration.

Figure 5a–d represents Boltzmann plots for Cu I lines (324.75, 327.39, 515.32, 521.82 nm) where the $\ln(I.\lambda/A_{ki}.g_k)$ is considered for each exciting level energy E_k at different L_λ, under a gradually increase laser pulse energy from 20 to 80 mJ, respectively. The slope of each relation can deduce the electron temperature from Eq. (2) with uncertainty of about ±10%, which mainly determined from the transition probabilities and emission line intensities (Qindeel and Tawfik 2014; Xu et al. 2019). The observed data from the Boltzmann plots are summarized in Table 2 with the linear fitting of R^2 (correlation coefficient value) for each of the laser pulse energies.

From Table 2, it can be found that the plasma plume temperature values range from about 10,000 to 20,000 K depend on the laser wavelength and pulse energy. At L_λ 1064, 532, 355 and 266 nm, the values of the plasma temperature increased from about 14,565 to 19,967 K, from 13,355 to 17,265 K, from 11,982 to 15,242 K and from 10,698 to 14,222 K due to a steep increase in the laser pulse energy from 20 to 80 mJ, respectively.

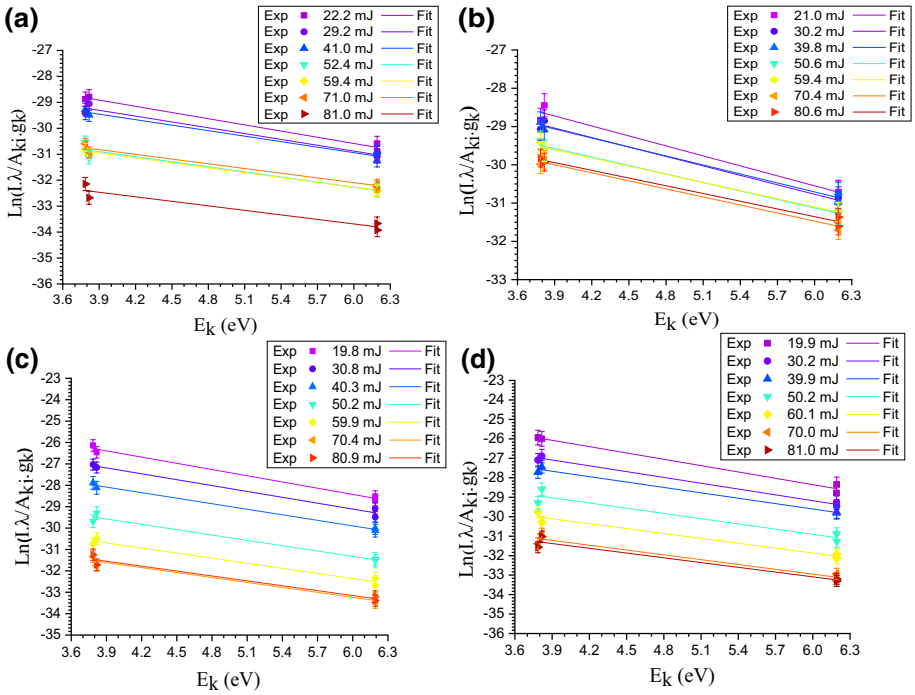

Fig. 5 A Boltzmann plots for the Cu I lines (324.75, 327.39, 515.32, 521.82 nm) at different laser pulse energies and different laser wavelengths **a** 1064 nm, **b** 532 nm, **c** 355 nm and **d** 266 nm

Table 2 Data analysis of the Boltzmann plots and the plasma plume temperature (T_e) at different laser pulse energies and laser wavelengths (L_λ) with correlation coefficient (R^2)

Laser pulse energy (mJ)	Laser wavelength											
	L_λ 1064 nm			L_λ 532 nm			L_λ 355 nm			L_λ 266 nm		
	Slope	T_e (K)	R^2	Slope	T_e (K)	R^2	Slope	T_e (K)	R^2	Slope	T_e (K)	R^2
20	−0.796	14,564.5	0.98	−0.869	13,354.4	0.98	−0.968	11,981.2	0.98	−1.084	10,697.8	0.98
30	−0.748	15,500.2	0.97	−0.823	14,095.7	0.99	−0.916	12,667.8	0.98	−0.994	11,664.5	0.99
40	−0.706	16,433.0	0.97	−0.782	14,823.1	0.98	−0.863	13,444.1	0.99	−0.923	12,569.0	0.99
50	−0.654	17,741.9	0.95	−0.740	15,669.7	0.99	−0.832	13,946.6	0.97	−0.893	12,985.3	0.94
60	−0.630	18,403.5	0.99	−0.709	16,358.8	0.99	−0.792	14,643.5	0.97	−0.839	13,817.1	0.96
70	−0.606	19,140.6	0.97	−0.700	16,571.4	0.98	−0.770	15,053.8	0.97	−0.826	14,047.9	0.95
80	−0.581	19,967.3	0.93	−0.672	17,264.2	0.98	−0.761	15,241.6	0.97	−0.815	14,221.7	0.96

Figure 6 demonstrates the variation of the Cu plasma temperature with the laser pulse energy at different L_λ, where the plasma temperature elevated with the laser pulse energy and wavelength which is agreement with previous works (Bogaerts and Chen 2005; Hoffman et al. 2011; Hussein et al. 2013). This increase of the plasma temperature with the laser pulse energy can be understood due to two reasons. Firstly, due to an increase in the mass-ablation rate (Hussain et al. 2016; Murbat 2017). Secondly, due to one of two interaction probabilities of a so-called ''plasma shielding'' (Cabalin and Laserna 1998; Bogaerts and Chen 2005), first, once a plasma is formed, a part of the laser beam is absorbed by the plasma, by electron-ion inverse-Bremsstrahlung or electron–neutral inverse-Bremsstrahlung, and second, by photo-ionization as a dominated interaction. The probability of electron-ion process is much greater than that by electron–neutral, except in the very early stages of the laser evaporation process, and thus electron–neutral is generally considered negligible during laser ablation processes (Bogaerts and Chen 2005; Hussein et al. 2013). The values of inverse-Bremsstrahlung absorption and the photo-ionization absorption coefficients α_{IB} and α_{PI} respectively, are given by a previous work (Chang and Warner 1996) as follows;

$$\alpha_{IB} = 1.37 \times 10^{-35} L_\lambda^3 N_e^2 T_e^{-1/2} \tag{3}$$

$$\alpha_{PI} = 7.9 \times 10^{18} \left(\frac{E_n}{h\nu}\right)^3 \left(\frac{I}{E_n}\right)^{1/2} \sum_n N_{e_n} \tag{4}$$

where L_λ is the laser wavelength in μm, T_e plasma electron temperature, E_n and N_e are the ionization energy and electron density of the excited state n, respectively; h is the Planck constant; ν is the laser frequency ($\nu = c/L_\lambda$) and I is the ionization potential of the ground state atom. According to Eqs. (3 and 4) at different laser wavelengths, it can be inferred that the inverse–Bremsstrahlung will be leading at 1064 nm (NIR) while photo-ionization will be the dominated absorption mechanism at 266 nm (UV) (Mao et al. 1998; Cowpe et al. 2011). Meanwhile, for picosecond pulse regime, it has been found that the plasma shielding retains a great impact on the process of ultrafast pulsed laser ablation, due to the inverse Bremsstrahlung most of the laser energy will be absorbed by the free electrons of the target, especially at higher laser fluence (Tan et al. 2018). The later retain more energetic electrons i.e. higher electron temperature and electron density with the increase of the

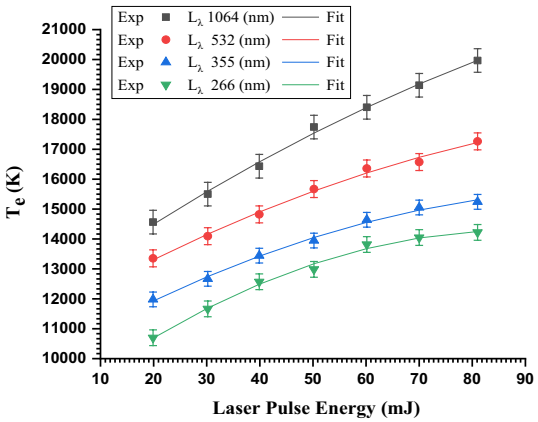

Fig. 6 The effect of different laser wavelengths (L_λ) and pulse energies on the Cu plasma temperature (T_e)

picosecond laser wavelength and pulse energy. These observed results are in good agreement with previous work by others (Hoffman et al. 2011; Hamad 2016; Tan et al. 2018).

3.3.2 Determination of the plasma electron density

In order to estimate the plasma electron density, we have considered the Stark-broadening profile of Cu I 324.75 and 327.39 nm. The fundamental line width $\Delta\lambda_{FWHM}$ is determined by deconvolution for each observed line profile as a Lorentz profile (Qindeel and Tawfik 2014; Asamoah and Hongbing 2017) using Origin software version 9.5 at fixed laser pulse energy at 40 mJ as represented in Figs. 7. Assuming LTE conditions as mentioned before, the electron density is considered by adopting Boltzmann distribution of the electron density as in following in Eq. (5) (Mohamed 2008; Mortazavi et al. 2014):

$$N_e \approx \left(\frac{\Delta\lambda_{FWHM}}{2W_e}\right) \times 10^{16} \tag{5}$$

where N_e is the electron density (in cm^{-3}), $\Delta\lambda_{FWHM}$ is the fundamental line width at half maximum and W_e is the electron impact parameter (Stark-broadening value). The average values of the W_e for Cu I 324.75 and 327.39 nm found from reference (Il'in 2003) as 0.00469 and 0.00406 nm, respectively. The Stark line width $\Delta\lambda_{FWHM}$ can be corrected by subtracting the instrumental $\Delta\lambda_{instrument}$ from the observed line width $\Delta\lambda_{observed}$ as follows:

$$\Delta\lambda_{FWHM} = \Delta\lambda_{observed} - \Delta\lambda_{instrument} \tag{6}$$

The observed values of the plasma electron density at different laser pulse energies from 20 to 80 mJ are shown in Fig. 8. It can be implied that the plasma electron density values which considered for the Cu emission lines are varied from about 2×10^{17} to 1.5×10^{18} cm^{-3} depending on the laser pulse energy and wavelength. The observed N_e values have been listed in Table 3.

It can be concluded from Table 3 that, the difference between the electron density values for Cu I 324.73 and 327.39 nm lines are just fractions of order magnitude which can be understood due to the fluctuations in W_e values for these Cu lines (Il'in 2003; Hoffman et al. 2011). At L_λ 1064, 532, 355 and 266 nm, the values of the plasma electron density increased from about 0.44×10^{18} to 1.55×10^{18} cm^{-3}, from 0.50×10^{18} to 1.47×10^{18} cm^{-3}, from 0.45×10^{18} to 1.24×10^{18} $cm^{-3}$and from 0.24×10^{18} to 1.21×10^{18} cm^{-3} due to a steep increase in the laser pulse energy from 20 to 80 mJ, respectively.

To verify the LTE condition, the criteria of minimum electron density, proposed by McWhirter relation (7), which consider the collisional processes are dominated over the radiative processes, has been considered as following (Liu et al. 1999; Mortazavi et al. 2014):

$$N_{(e)} \geq 1.6\times10^{12} \times \Delta E^3 \times T_e^{(1/2)} \tag{7}$$

where ΔE is the highest energy difference between the upper and the lower energy level (eV) and T_e is the plasma temperature (K). The Cu emission spectral line 324.73 nm is the highest energy difference line as given in Table 1. According to R.H.S of relation (7), the N_e considered for Cu I 324.73 nm, where ΔE is 3.816 eV and the max T_e is 19,967.25 K which gives N_e value of 1.25×10^{16} cm^{-3}. On the other hand, the observed electron density values the Cu lines were in the range of 10^{18} cm^{-3} as shown in Fig. 8 and Table 3. Thus,

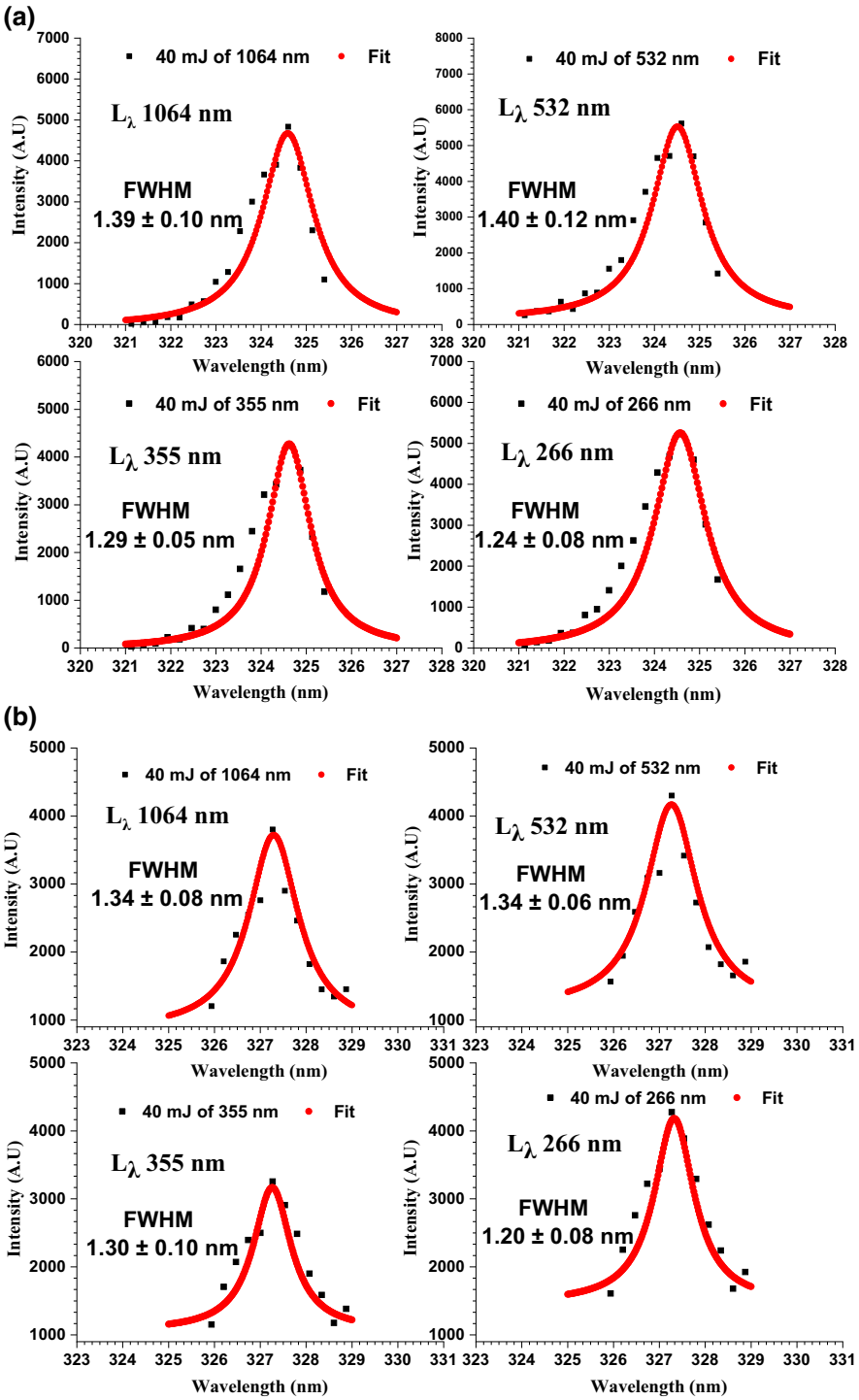

Fig. 7 Line profile of Cu I lines at **a** 324.73 nm and **b** 327.39 nm fitted with Lorentz function using Origin software version 9.5 at fixed laser pulse energy 40 mJ for different laser wavelengths (L_λ)

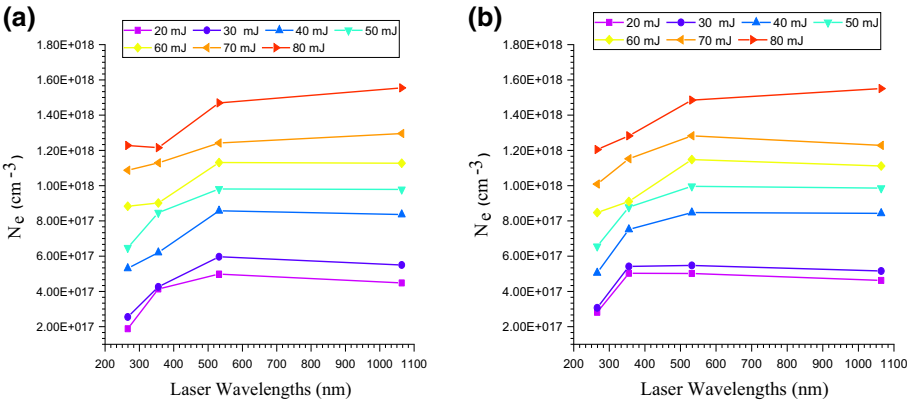

Fig. 8 The dependence of the plasma electron density (N_e) on the laser wavelength (L_λ) at 40 mJ (±5%) for Cu I lines **a** 324.73 nm and **b** 327.39 nm

Table 3 Data analysis of the plasma plume electron density (N_e) at different laser pulse energies and laser wavelengths (L_λ)

Laser pulse energy (mJ)	Laser wavelengths							
	L_λ 1064 nm		L_λ 532 nm		L_λ 355 nm		L_λ 266 nm	
	$N_e \times 10^{18}$ (cm^{-3}) at		$N_e \times 10^{18}$ (cm^{-3}) at		$N_e \times 10^{18}$ (cm^{-3}) at		$N_e \times 10^{18}$ (cm^{-3}) at	
	324.73 nm	327.39 nm	324.73 nm	327.39 nm	324.73 nm	327.39 nm	324.73 nm	327.39 nm
20	0.447	0.448	0.498	0.501	0.413	0.502	0.188	0.281
30	0.549	0.515	0.596	0.547	0.425	0.542	0.255	0.307
40	0.836	0.843	0.857	0.847	0.620	0.751	0.530	0.505
50	0.978	0.985	0.981	0.996	0.846	0.878	0.647	0.655
60	1.127	1.111	1.131	1.147	0.901	0.910	0.883	0.847
70	1.295	1.230	1.241	1.282	1.129	1.152	1.087	1.008
80	1.554	1.550	1.469	1.485	1.215	1.282	1.227	1.204

relation (7) is valid which indicates that the studied plasma can be considered in the LTE condition.

4 Conclusion

This work investigated the effects of a picosecond laser wavelength and pulse energy variations on the observed copper plasma characterizations using the LIPS technique. It has been observed that, the copper emission lines intensities (S/N), plasma temperature and density have shown strong dependence on laser wavelength and pulse energy. Both of ion inverse-Bremsstrahlung and photo-ionization absorption mechanisms are considered for the interaction shielding mechanisms with the copper surface and plasma. Using picosecond pulses enhances the plasma shielding due to the inverse Bremsstrahlung as dominant absorption mechanism over photo-ionization. So that, most of the laser energy would be absorbed by the free electrons of the target, especially at higher laser fluence and preserve

more energetic electrons i.e. increase the electron temperature and the electron density with the increase of the picosecond laser wavelength and pulse energy. These effects can explain the observed increase of electron temperature and density values by increasing the laser wavelength from 266 up to 1064 nm.

The obtained results confirmed that, by controlling the picosecond laser pulse parameters the observed copper plasma temperature can be tuned from around 10,000 to 20,000 K and the plasma density can be tuned from about 2×10^{17} to 1.5×10^{18} cm^{-3}, which may be applied to partial control of the plasma interaction dynamics in the spectroscopic analysis of the material sciences.

References

Abdellatif, G., Imam, H.: A study of the laser plasma parameters at different laser wavelengths. Spectrochim. Acta-Part B At. Spectrosc. **57**, 1155–1165 (2002). https://doi.org/10.1016/S0584-8547(02)00057-5

Adhikari, B.R., Khanal, R.: Introduction to the plasma state of matter. Himal. Phys. **4**, 60–64 (2013). https://doi.org/10.3126/hj.v4i0.9430

Asamoah, E., Hongbing, Y.: Influence of laser energy on the electron temperature of a laser-induced Mg plasma. Appl. Phys. B Lasers Opt. **123**, 1–6 (2017). https://doi.org/10.1007/s00340-016-6617-3

Asenjo-Castillo, J., Vargas-Blanco, I.: Espectroscopia de Plasmas en condiciones de presión atmosférica. Rev. Tecnol. en Marcha **29**, 47 (2016). https://doi.org/10.18845/tm.v29i6.2901

Aslam Farooq, W., Tawfik, W., Al-Mutairi, F.N., Alahmed, Z.A.: Qualitative analysis and plasma characteristics of soil from a desert area using LIBS technique. J. Opt. Soc. Korea. **17**, 548–558 (2013). https://doi.org/10.3807/JOSK.2013.17.6.548

Baskevicius, A., Balachninaite, O., Karpavicius, M., Butkus, S., Paipulas, D., Sirutkaitis, V.: Monitoring of the femtosecond laser micromachining process of materials immersed in water by use of laser-induced breakdown spectroscopy. J. Laser Micro Nanoeng. **11**, 381–387 (2016). https://doi.org/10.2961/jlmn.2016.03.0018

Bogaerts, A., Chen, Z.: Effect of laser parameters on laser ablation and laser-induced plasma formation: A numerical modeling investigation. Spectrochim. Acta Part B At. Spectrosc. **60**, 1280–1307 (2005). https://doi.org/10.1016/j.sab.2005.06.009

Cabalin, L.M., Laserna, J.J.: Experimental determination of laser induced breakdown thresholds of metals under nanosecond Q-switched laser operation. Spectrochim. Acta Part B At. Spectrosc. **53**, 723–730 (1998). https://doi.org/10.1016/S0584-8547(98)00107-4

Chang, J.J., Warner, B.E.: Laser-plasma interaction during visible-laser ablation of methods. Appl. Phys. Lett. **69**, 473–475 (1996). https://doi.org/10.1063/1.118144

Conrads, H., Schmidt, M.: Plasma generation and plasma sources. Plasma Sources Sci. Technol. **9**, 441–454 (2000). https://doi.org/10.1088/0963-0252/9/4/301

Cooper, J.: Plasma spectroscopy. Rep. Prog. Phys. **29**, 302 (1966). https://doi.org/10.1088/0034-4885/29/1/302

Cowpe, J.S., Moorehead, R.D., Moser, D., Astin, J.S., Karthikeyan, S., Kilcoyne, S.H., Crofts, G., Pilkington, R.D.: Hardness determination of bio-ceramics using laser-induced breakdown spectroscopy. Spectrochim. Acta Part B At. Spectrosc. **66**, 290–294 (2011). https://doi.org/10.1016/j.sab.2011.03.007

Ding P., Hu B., Li Y.: Numerical simulation of copper ablation by ultrashort laser pulses,17, pp. 10–12 (2011)

Dong, Y., Wang, K., Tan, Y., Wang, Q., Li, J., Mark, H., Zhang, S.: Synthesis and Characterization of Pure Copper Nanostructures Using Wood Inherent Architecture as a Natural Template. Nanoscale Res. Lett. **13**, 119 (2018). https://doi.org/10.1186/s11671-018-2543-0

Eddington, A.S.: The Internal Constitution of the Stars. Cambridge University Press, Cambridge (1988)

Fantz, U.: Basics of plasma spectroscopy. Plasma Sources Sci. Technol. **15**, S137–S147 (2006). https://doi.org/10.1088/0963-0252/15/4/S01

Fornarini, L., Spizzichino, V., Colao, F., Fantoni, R., Lazic, V.: Influence of laser wavelength on LIBS diagnostics applied to the analysis of ancient bronzes. Anal. Bioanal. Chem. **385**, 272–280 (2006). https://doi.org/10.1007/s00216-006-0300-1

Gojani, A.B.: Experimental study of laser-induced brass and copper plasma for spectroscopic applications. ISRN Spectrosc. **2012**, 1–8 (2012). https://doi.org/10.5402/2012/868561

Gondal, M.A., Dastageer, M.A.: Elemental analysis of soils by laser induced breakdown spectroscopy. Springer Ser. Opt. Sci. **182**, 293–308 (2014). https://doi.org/10.1007/978-3-642-45085-3_11
Hamad, A.H.: Effects of different laser pulse regimes (nanosecond, picosecond and femtosecond) on the ablation of materials for production of nanoparticles in liquid solution. High Energy Short Pulse Lasers (2016). https://doi.org/10.5772/63892
Hoffman, J., Moscicki, T., Szymanski, Z.: The effect of laser wavelength on heating of ablated carbon plume. Appl. Phys. A Mater. Sci. Process. **104**, 815–819 (2011). https://doi.org/10.1007/s00339-011-6420-2
Hussain, T., Gondal, M.A., Shamraiz, M.: Determination of plasma temperature and electron density of iron in iron slag samples using laser induced breakdown spectroscopy. In: IOP Conf. Ser. Mater. Sci. Eng. 146 (2016). https://doi.org/10.1088/1757-899X/146/1/012017
Hussein, A.E., Diwakar, P.K., Harilal, S.S., Hassanein, A.: The role of laser wavelength on plasma generation and expansion of ablation plumes in air. J. Appl. Phys. **113**, 143305 (2013). https://doi.org/10.1063/1.4800925
Il'in, G.G.: The estimation of Stark broadening parameters of the neutral copper atoms resonance spectral lines by the parameters of asymmetric self-reversed profiles. 156–159 (2003). https://doi.org/10.1063/1.1370610
Jarota, A., Pastorczak, E., Tawfik, W., Xue, B., Kania, R., Abramczyk, H., Kobayashi, T.: Exploring the ultrafast dynamics of a diarylethene derivative using sub-10 fs laser pulses. Phys. Chem. Chem. Phys. **21**, 192–204 (2019). https://doi.org/10.1039/c8cp05882b
Killian, T.C., Rolston, S.L.: Ultracold neutral plasmas. Phys. Today. **63**, 46–51 (2010). https://doi.org/10.1063/1.3366240
Kompitsas, M., Bassiotis, I., Diamantopoulou, A., Giannoudakos, A., Ave, V.K.: Laser induced plasma spectroscopy (lips) as an efficient method for elemental analysis of environmental samples. EARSeL eProceedings. 130–138 (2000)
Kramida, A., Ralchenko, Y.: NIST At. Spectra Database. National Institute of Standards and Technology, Gaithersburg, MD (2019). https://doi.org/10.18434/T4W30F
Liu, H.C., Mao, X.L., Yoo, J.H., Russo, R.E.: Early phase laser induced plasma diagnostics and mass removal during single-pulse laser ablation of silicon. Spectrochim. Acta Part B At. Spectrosc. **54**, 1607–1624 (1999). https://doi.org/10.1016/S0584-8547(99)00092-0
Mao, X.L., Borisov, O.V., Russo, R.E.: Enhancements in laser ablation inductively coupled plasma-atomic emission spectrometry based on laser properties and ambient environment. Spectrochim. acta. Part B At. Spectrosc. **53**, 731–739 (1998). https://doi.org/10.1016/S0584-8547(98)00106-2
Messaoud Aberkane, S., Bendib, A., Yahiaoui, K., Abdelli-Messaci, S., Amara, S.E., Harith, M.A.: Effect of laser wavelength on the correlation between plasma temperature and surface hardness of Fe-V-C metallic alloys. Spectrochim. Acta Part B At. Spectrosc. **113**, 147–151 (2015). https://doi.org/10.1016/j.sab.2015.09.012
Mohamed, W.T.Y.: Improved LIBS limit of detection of Be, Mg, Si, Mn, Fe and Cu in aluminum alloy samples using a portable Echelle spectrometer with ICCD camera. Opt. Laser Technol. **40**, 30–38 (2008). https://doi.org/10.1016/j.optlastec.2007.04.004
Mortazavi, S.Z., Parvin, P., Mousavi Pour, M.R., Reyhani, A., Moosakhani, A., Moradkhani, S.: Time-resolved evolution of metal plasma induced by Q-switched Nd:YAG and ArF-excimer lasers. Opt. Laser Technol. **62**, 32–39 (2014). https://doi.org/10.1016/j.optlastec.2014.02.006
Naeem, M.A., Iqbal, M., Amin, N., Musadiq, M., Jamil, Y., Cecil, F.: Measurement of electron density and temperature of laser-induced copper plasma. Asian J. Chem. **25**, 2192–2198 (2013)
Phillips, K.C., Gandhi, H.H., Mazur, E., Sundaram, S.K.: Ultrafast laser processing of materials: a review. Adv. Opt. Photonics. **7**, 684 (2015). https://doi.org/10.1364/aop.7.000684
Qindeel, R., Tawfik, W.: Measurement of plasma characteristics of the optically generated copper plasma by laser spectroscopy technique. Optoelectron. Adv. Mater. Rapid Commun. **8**, 741–746 (2014)
Rusak, D.A., Castle, B.C., Smith, B.W., Winefordner, J.D.: Fundamentals and applications of laser-induced breakdown spectroscopy. https://www.tandfonline.com/doi/abs/10.1080/10408349708050587 (1997)
Safeen, A., Shah, W.H., Khan, R., Shakeel, A., Iqbal, Y., Asghar, G., Khan, R., Khan, G., Safeen, K., Shah, W.H.: Measurement of plasma parameters for copper using laser induced breakdown spectroscopy. Dig. J. Nanomater. Biostruct. **14**, 29–35 (2019)
Sahai, A., Goswami, N., Kaushik, S.D., Tripathi, S.: Cu/Cu2O/CuO nanoparticles: novel synthesis by exploding wire technique and extensive characterization. Appl. Surf. Sci. **390**, 974–983 (2016). https://doi.org/10.1016/J.APSUSC.2016.09.005
Sugioka, K.: Progress in ultrafast laser processing and future prospects. Nanophotonics. **6**, 393–413 (2017). https://doi.org/10.1515/nanoph-2016-0004

Tan, S., Wu, J., Zhang, Y., Wang, M., Ou, Y.: A model of ultra-short pulsed laser ablation of metal with considering plasma shielding and non-fourier effect. Energies. **11**, 3163 (2018). https://doi.org/10.3390/en11113163

Tawfik, W.: Precise measurement of ultrafast laser pulses using spectral phase interferometry for direct electric-field reconstruction. J. Nonlinear Opt. Phys. Mater. **24**, 1550040 (2015). https://doi.org/10.1142/S021886351550040X

Thiem, T.L., Salter, R.H., Gardner, J.A., Lee, Y.I., Sneddon, J.: Quantitative simultaneous elemental determinations in alloys using laser-induced breakdown spectroscopy (libs) in an ultra-high vacuum. Appl. Spectrosc. **48**, 58–64 (1994). https://doi.org/10.1366/0003702944027615

Unnikrishnan, V.K., Alti, K., Kartha, V.B., Santhosh, C., Unnikrishnan, V.K., Kamlesh Alti, Kartha, V.B., Santhosh, C., Gupta, G.P., Suri, B.M.: Measurements of plasma temperature and electron density in laser-induced copper plasma by time-resolved spectroscopy of neutral atom and ion emissions. Pramana Jour. Pramana – J. Phys. **74**, 983–993 (2010)

Xu, W., Chen, A., Wang, Q., Zhang, D., Wang, Y., Li, S., Jiang, Y., Jin, M.: Generation of high-temperature and low-density plasma with strong spectral intensity by changing the distance between the focusing lens and target surface in femtosecond laser-induced breakdown spectroscopy. J. Anal. At. Spectrom. **34**, 1018–1025 (2019). https://doi.org/10.1039/c8ja00359a

Terms and Conditions

Springer Nature journal content, brought to you courtesy of Springer Nature Customer Service Center GmbH ("Springer Nature").

Springer Nature supports a reasonable amount of sharing of research papers by authors, subscribers and authorised users ("Users"), for small-scale personal, non-commercial use provided that all copyright, trade and service marks and other proprietary notices are maintained. By accessing, sharing, receiving or otherwise using the Springer Nature journal content you agree to these terms of use ("Terms"). For these purposes, Springer Nature considers academic use (by researchers and students) to be non-commercial.

These Terms are supplementary and will apply in addition to any applicable website terms and conditions, a relevant site licence or a personal subscription. These Terms will prevail over any conflict or ambiguity with regards to the relevant terms, a site licence or a personal subscription (to the extent of the conflict or ambiguity only). For Creative Commons-licensed articles, the terms of the Creative Commons license used will apply.

We collect and use personal data to provide access to the Springer Nature journal content. We may also use these personal data internally within ResearchGate and Springer Nature and as agreed share it, in an anonymised way, for purposes of tracking, analysis and reporting. We will not otherwise disclose your personal data outside the ResearchGate or the Springer Nature group of companies unless we have your permission as detailed in the Privacy Policy.

While Users may use the Springer Nature journal content for small scale, personal non-commercial use, it is important to note that Users may not:

1. use such content for the purpose of providing other users with access on a regular or large scale basis or as a means to circumvent access control;
2. use such content where to do so would be considered a criminal or statutory offence in any jurisdiction, or gives rise to civil liability, or is otherwise unlawful;
3. falsely or misleadingly imply or suggest endorsement, approval , sponsorship, or association unless explicitly agreed to by Springer Nature in writing;
4. use bots or other automated methods to access the content or redirect messages
5. override any security feature or exclusionary protocol; or
6. share the content in order to create substitute for Springer Nature products or services or a systematic database of Springer Nature journal content.

In line with the restriction against commercial use, Springer Nature does not permit the creation of a product or service that creates revenue, royalties, rent or income from our content or its inclusion as part of a paid for service or for other commercial gain. Springer Nature journal content cannot be used for inter-library loans and librarians may not upload Springer Nature journal content on a large scale into their, or any other, institutional repository.

These terms of use are reviewed regularly and may be amended at any time. Springer Nature is not obligated to publish any information or content on this website and may remove it or features or functionality at our sole discretion, at any time with or without notice. Springer Nature may revoke this licence to you at any time and remove access to any copies of the Springer Nature journal content which have been saved.

To the fullest extent permitted by law, Springer Nature makes no warranties, representations or guarantees to Users, either express or implied with respect to the Springer nature journal content and all parties disclaim and waive any implied warranties or warranties imposed by law, including merchantability or fitness for any particular purpose.

Please note that these rights do not automatically extend to content, data or other material published by Springer Nature that may be licensed from third parties.

If you would like to use or distribute our Springer Nature journal content to a wider audience or on a regular basis or in any other manner not expressly permitted by these Terms, please contact Springer Nature at

onlineservice@springernature.com